


Article

Intracrystalline Reaction-Induced Cracking in Olivine Evidenced by Hydration and Carbonation Experiments

Romain Lafay ^{1,*}, German Montes-Hernandez ², François Renard ^{2,3}  and Pierre Vonlanthen ¹

¹ Institute of Earth Sciences, University of Lausanne, 1015 c Géopolis, Switzerland; pierre.vonlanthen@unil.ch

² University of Grenoble Alpes, University of Savoie Mont Blanc, CNRS, IRD, IFSTTAR, ISTerre, 38000 Grenoble, France; german.montes-hernandez@univ-grenoble-alpes.fr (G.M.-H.); francois.renard@geo.uio.no (F.R.)

³ The Njord Centre, Physics of Geological Processes, Department of Geosciences, University of Oslo, Box 1048, Blindern, 0316 Oslo, Norway

* Correspondence: romain.lafay@unil.ch; Tel.: +41-21-692-35-18

Received: 3 August 2018; Accepted: 14 September 2018; Published: 18 September 2018



Abstract: In order to better understand the microtextural changes associated with serpentinization reactions, natural millimeter-sized olivine grains were experimentally reacted with alkaline NaOH and NaHCO₃ solutions at a temperature of 200 °C and for durations of 3 to 12 months. During hydration experiments, dissolution and precipitation were intimately correlated in time and space, with reaction products growing in situ, either as layered veins or as nearly continuous surface cover. In contrast, carbonation experiments showed a strong decoupling between both processes leading to essentially delocalized precipitation of the reaction products away from dissolution sites. Textural analyses of the samples using scanning electron microscopy, Raman spectroscopy, and X-ray synchrotron microtomography provided experimental evidence for a cause-and-effect relationship between in situ precipitation and intracrystalline reaction-induced cracking in olivine. Juvenile cracks typically nucleated at the tip of dissolution notches or on diamond-shaped pores filled with reaction products, and propagated through the olivine crystal lattice during the course of the reaction. The occurrence of new cracks at the tip of diamond-shaped pores, but also of tiny subspherical pores lining up along microcracks, indicated that fracturation and porosity networks were mutually driven, making serpentinization an extremely efficient alteration process over time. Alternatively, our data suggested that some form of porosity also developed in absence of fracturation, thus further highlighting the remarkable efficiency and versatility of serpentinization processes.

Keywords: serpentinization; hydration; carbonation; reaction-induced cracking; veining; porosity; X-ray synchrotron microtomography

1. Introduction

Serpentinization and carbonation of ultramafic rocks is a ubiquitous process within the oceanic lithosphere, which results in intense rock alteration and widespread redistribution of chemical elements. Over the last few years, ultramafic rocks alteration reactions have been the subject of growing interests among scientists, firstly because they significantly influence rock rheology [1] and volatile recycling [2], but also because they raise realistic societal and environmental expectations, e.g., in the search for long-term carbon dioxide sequestration strategies [3,4] or for a source of renewable H₂ [5].

Serpentinization is a hydration reaction during which olivine ((Mg,Fe)SiO₄) is transformed into serpentine ((Mg,Fe)₃Si₂O₅(OH)₃), along with a limited number of additional phases. The composition of aqueous fluids, and in particular the presence of carbon dioxide (CO₂) among the volatile phases,

plays an important role in the determination of mineral species in the reaction products. In the absence of carbon dioxide, serpentine is typically accompanied by brucite ((Mg,Fe)(OH)₂). In contrast, when carbon dioxide is present, a carbonation reaction occurs leading to the formation of magnesite (MgCO₃), dolomite (CaMg(CO₃)₂), or calcite (CaCO₃). In addition to hydration and carbonation, serpentinization involves redox reactions during which divalent iron is oxidized and incorporated into serpentine and an oxide phase, typically magnetite (Fe₃O₄) or hematite (Fe₂O₃). The alteration of olivine through serpentinization is accompanied by a significant increase in the rock volume, with differences of up to 50% between the molar volumes of the starting minerals and the reaction products [6,7].

Serpentinization is directly dependent on the ability of aqueous fluids to percolate towards the reaction fronts. Therefore, the evolution of rock total porosity over time is one of the key features of serpentinization reactions. This is a nontrivial issue, especially in a context where the increase in volume associated with phase transformations tends to form veins, obstructing circulation pathways, which may in turn impede fluid flow and inhibit the reaction [8,9]. However, even if serpentinization is in theory self-limiting in essence, the large bodies of fully serpentinized rocks outcropping in various geological settings around the world [9,10] indicate that situations of pervasive and sustained fluid flow may persist for long periods of time. For that to happen, pre-existing fluid circulation pathways have to remain open, and/or new ones have to be created in the course of the reaction [10]. In the former case, significant mass transfer is required between dissolution and precipitation sites [7,11,12], while the latter is achieved through rock fracturing [9,10] or the build-up of interconnected porosity [10,13]. Even if those features are well established and corroborated by various field observations e.g., [14,15] and in laboratory experiments e.g., [16,17], the mechanisms at play and the conditions under which they occur are still not well constrained. For instance, several processes have been utilized to account for the pervasive rock fracturation observed during serpentinization. These include mechanisms not directly related to the reaction itself, such as thermal cracking of olivine upon cooling [18] and fracturing resulting from local tectonic stresses [19]. More recently, an intrinsic mechanism of reaction-induced cracking, possibly triggered by the major volume increase associated with phase transformations, has been put forward [8,20]. While there are recent convincing experimental evidence for the occurrence of intercrystalline reaction-induced cracking [13,21], equivalent data supporting the existence of intracrystalline reaction-induced cracking is still lacking. In addition, other critical issues such as the role of carbon dioxide in dissolution-precipitation mechanisms, or the mutual evolution and interdependence of fracturation and porosity networks are important topics that remain to be investigated further.

Most of the recent experimental studies dealing with flow-through [20,22], and static [23] alteration of natural peridotites were faced with the challenge of slow reaction rates. To overcome this issue, many of the experimental studies were performed under static confined pressure using either fine grain (<<100 μm) starting materials [17,24–27], or sintered olivine grains [13,26] or thermally cracked samples [16]. While the large surface area associated with smaller grain sizes may enhance reaction kinetics, it may also hinder key processes typically occurring in coarser-grained natural rocks. For instance, the occurrence of intracrystalline reaction-induced cracking and the development of interconnected porosity may be hampered or biased in fine-grained materials by the wealth of readily available interfaces. To avoid these effects and to allow for a more realistic comparison with the textures observed in natural serpentinites, here we have decided to use larger olivine grains (>1 mm) as starting materials. The experiments have been carried out for 3 to 12 months at a temperature of 200 °C and vapor saturated pressure. Alkaline aqueous solutions have been used as reactive fluids in a setup simulating no fluid flow and static conditions. The present study reports the first experimental evidence for intracrystalline reaction-induced cracking in olivine during serpentinization, and clearly demonstrates the critical role played by carbon dioxide in the degree of coupling between dissolution and precipitation reactions. We also report new findings on the creation and evolution of porosity over time, in particular on the ability of the system to develop porosity in the absence of fracturation.

2. Materials and Methods

2.1. Sample Preparation and Experimental Conditions

Serpentinization experiments were conducted at the ISTERre laboratory of the University of Grenoble Alpes (Grenoble, France). The starting material consisted of fresh natural olivine grains of unknown origin, 1 to 5 mm in size (Figure 1). This choice was motivated firstly because this size range is observed in many peridotite rocks, and secondly because these olivine grains had a chemical composition similar to the well-documented San Carlos olivine (see Supplementary Materials S1). The grains contained a few mineral inclusions of clinopyroxene and orthopyroxene and showed very little porosity or fracturation. Sample preparation involved washing in concentrated 3 M HCl solution for 1 to 2 min to remove any surface contaminants, followed by rinsing in deionized water. No thermally induced cracking of the grains was applied.

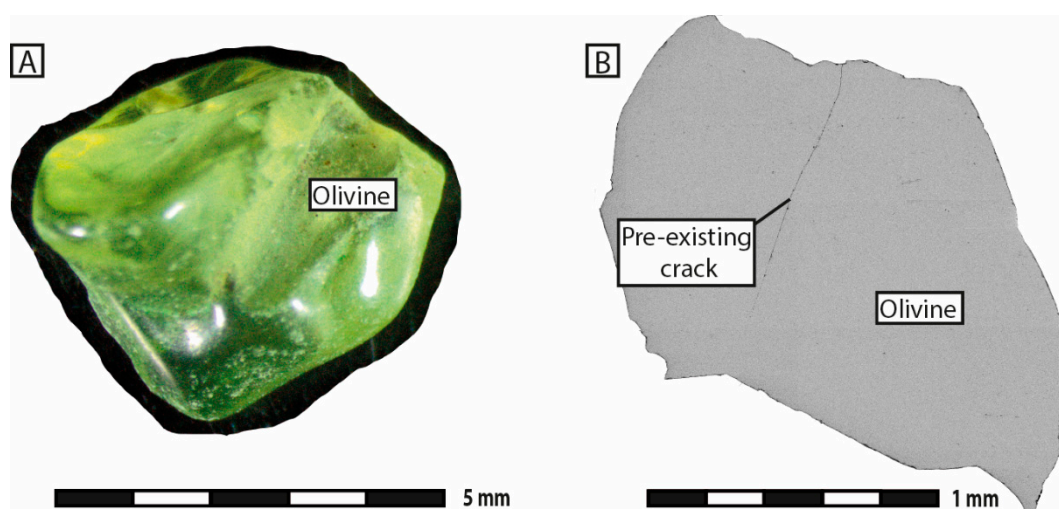


Figure 1. (A) Optical micrograph and (B) Backscattered electrons (BSE) image of an olivine grain before starting the experiments.

The selected olivine grains were divided into two groups, each being reacted with a different aqueous solution, namely (i) a highly alkaline 1 M NaOH solution to induce hydration of the grains, and (ii) a mildly alkaline NaHCO₃ solution to induce carbonation of the grains. These solutions were selected as reactants because of their ability to generate a wide spectrum of alteration features similar to those observed in nature during serpentinization reactions, and additionally because they significantly enhanced reaction kinetics [14,15], thus keeping the experiments within realistic time frames. This choice was also well in line with previous observations reporting the enhancing effect of alkaline fluids on the rate of serpentinization reactions [24], and the well-established increase in fluid alkalinity over time [28].

At the beginning of the experiments, four to ten olivine grains (~200 mg) along with 2 mL of solution were put in a static-batch Teflon capsule fitted into a closed steel autoclave (see Supplementary Materials S2). The choice of such a high solution-to-mineral ratio (~10) was justified to avoid major changes in the composition of the solution as the reaction proceeded. Experimental runs were conducted for durations of 3, 6 and 12 months at a temperature of 200 °C (Table 1), which is considered a relevant temperature value for both hydration and carbonation of ultramafic rocks [29,30]. At the end of the experiments, the autoclaves were quenched in cold water to stop the reaction and freeze the reaction products. The samples were then rinsed and oven-dried at 60 °C for 24 h.

Table 1. Experimental conditions.

Run #	Duration (months)	Temperature (°C)	Solute Type	Reactive Aqueous Solution			
				Volume (mL)	pH		Quenched 25 °C
					25 °C	200 °C ^γ	
1	3	200	NaOH ^α	2	13.5	11.0	13.4
2	6	200	NaOH ^α	2	13.5	11.0	13.3
3	12	200	NaOH ^α	2	13.5	11.0	13.3
4	3	200	NaHCO ₃ ^β	2	8.7	7.4	9.2
5	6	200	NaHCO ₃ ^β	2	8.7	7.4	9.3
6	12	200	NaHCO ₃ ^β	2	8.7	7.4	9.3

^α The NaOH (1 M) solution was obtained by dissolving 40 g of NaOH into 1 L of deionized water. ^β The NaHCO₃ solution (0.95 M of total carbon) was obtained by ionic dissociation of dissolved CO₂ in concentrated 2 M NaOH solution (See [29] for more details). ^γ pH calculated at 200 °C using the PHREEQC software.

In addition, a seventh experiment was run on similar olivine grains using high-purity deionized water as a reactive solution (See Supplementary Materials S2). This experiment was carried out for a duration of 12 months at a temperature of 200 °C. The observed features served as references to attest to the validity of the serpentinization experiments performed under alkaline conditions.

2.2. Scanning Electron Microscopy (SEM) and Energy Dispersive Spectroscopy (EDS)

Reacted olivine grains and slurry residues were imaged at the Institute of Earth Sciences of the University of Lausanne (Lausanne, Switzerland) using a Tescan Mira II LMU Schottky field emission-scanning electron microscope (FE-SEM) operated at an acceleration voltage of 20 kV and a probe current of ~0.5 nA. The goal here was to identify mineral phases and textures, with a particular emphasis on the reaction products, porosity and fracturation. Backscattered electron (BSE) images were taken on finely-polished epoxy mounts coated with a 15 nm carbon layer, while a few olivine grains were hand-picked on aluminum stubs and gold-coated for secondary electron (SE) imaging.

Energy dispersive spectroscopy (EDS) analyses were carried out at the same facility to determine the chemical composition of the reaction products. This data was complemented by elemental maps on specific user-defined areas, in order to visualize the spatial distribution of key chemical elements, such as Si, Fe and Mg.

2.3. Raman Spectroscopy

In-situ Raman spectroscopy was used to differentiate the serpentine polymorphs chrysotile and lizardite, as they are characterized by distinct Raman peaks on the OH stretching range, with a single band at 3697 cm⁻¹, and two bands at 3682 cm⁻¹ and 3704 cm⁻¹, respectively. Raman spectra of the reaction products were collected using a Horiba LabRam HR800 (Jobin-Yvon Technologies) apparatus generating an argon laser beam, 532 nm in wavelength. Measurements were performed at the Institute of Earth Sciences of the University of Lausanne (Lausanne, Switzerland). The instrument was equipped with an Olympus™ BX30 open microscope used for fine focusing of the laser beam on the sample surface (probe size <1 μm in diameter). The reflected Raman signal was sampled for 60 s in two cycles, and analyzed using a 600 lines/mm grating.

2.4. X-ray Synchrotron Microtomography

The 3D morphologies of olivine grains were investigated using X-ray microtomography images acquired at the beamline ID19 of the European Synchrotron Radiation Facility in Grenoble (France). The main advantages of synchrotron microtomography over standard desktop micro-computed tomography alternatives include better spatial resolution and limited beam hardening artefacts due to the use of highly-coherent monochromatic X-ray radiation. The instrumentation was operated at

an energy of 35 keV and the setting was adjusted to image either X-ray absorption or phase contrast. Radiographs were taken over 360° at 0.18° intervals, all having a 16-bit grayscale depth and 2.2 μm pixel size. Cross-sectional tomographic slices and 3D volume renderings were then reconstructed and post-processed using the commercial AvizoFire™ software 9.4.

3. Results

3.1. Serpentinization Experiments in NaOH Solution

Experiments performed in NaOH solution resulted in major compositional and textural changes of the starting material. While the original olivine grains displayed pristine olive-green surfaces free of dissolution and secondary growth features, reacted grains showed a fibrous surface cover, mostly whitish to pale-green under the optical microscope (Figure 2). Despite the intense phase transformation that obviously took place, none of the grains broke up into individual fragments during the reactions in NaOH solution.

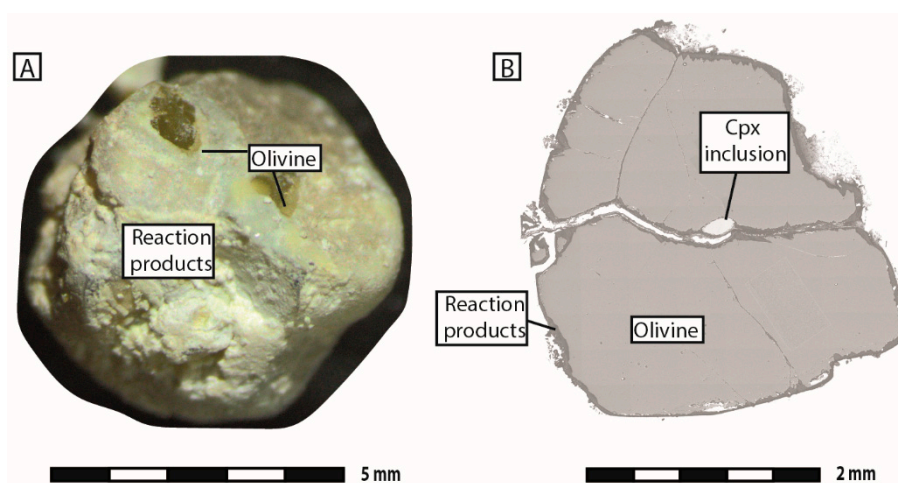


Figure 2. (A) Optical micrograph and (B) BSE image of an olivine grain after six months of reaction in NaOH solution (run # 2). Note the external and internal changes in texture with respect to the starting olivine grain shown in Figure 1. Cpx: clinopyroxene.

More detailed surface features typical for serpentinization reactions were identified under the SEM (Figure 3). After three months of reaction, serpentine flakes, a few tens of micrometres in thickness, grew on the external surface of the olivine grains and progressively spread out as the reaction progressed. When still visible, the olivine surface was generally rugged or mammillated. Selective dissolution on specific crystal faces resulted in the formation of closely spaced etch pits, which lined up and coalesced to form interconnected pit trails. After 6 to 12 months of reaction, chrysotile fibers arranged in bunches of tepee-like or spiral-shaped bundles (Figure 3e). The chrysotile cover sometimes formed a sub-regular array of 5- to 8-sided polygons, 10 to 50 μm in size, delimited by straight ridges (Figure 3f). This feature, typical for competitive growth, is often referred to as Voronoi tessellation in the literature [31]. As for etching, polygonization of the chrysotile cover was limited to specific olivine crystal faces.

Underneath the chrysotile cover, the serpentinization reaction led to the formation of an alteration rim, 10 to 150 μm thick, made of lizardite and brucite (Figure 3 and Supplementary Materials S2). Lizardite consisted of relatively homogeneous and dense aggregates of crystallites, making up most of the reaction volume. Brucite formed large euhedral crystals, up to 100 μm in size, located in direct contact with healthy olivine. Porosity was widespread within the outer 20 μm of the reaction rim but drastically decreased towards the interface with olivine. The reaction front was populated with numerous V-shaped dissolution notches, which sometimes formed corrugated or saw-tooth patterns when observed in polished sections (Figure 3g).

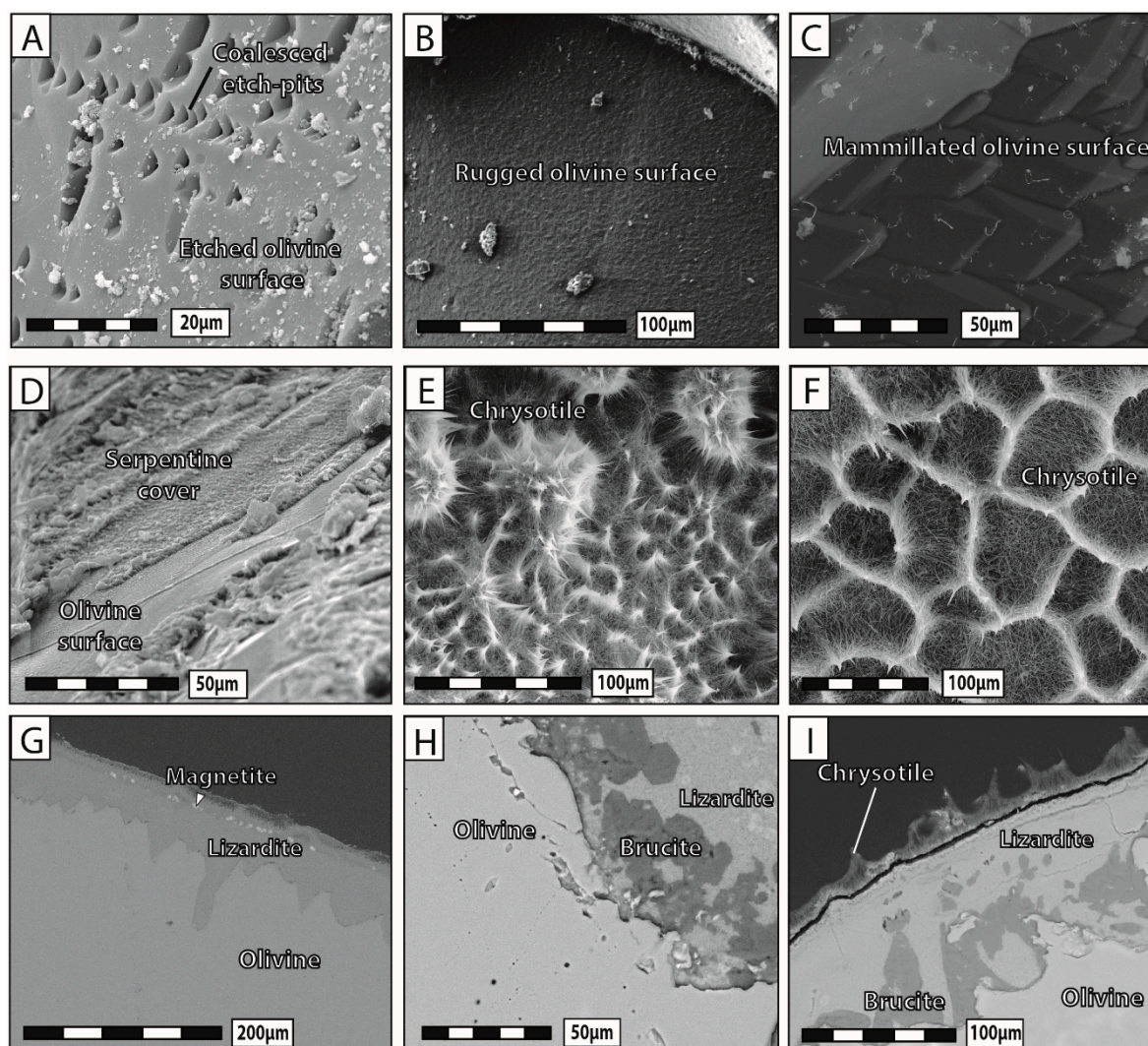


Figure 3. Scanning electron microscope (SEM) images of surface features after reaction in NaOH solution. (A) Selective dissolution resulting in closely spaced or coalesced etch pits. (B) Rugged and (C) mammillated olivine surface. (D) Lizardite growing onto fresh olivine. (E) Bunches of tepee-like chrysotile bundles. (F) Polygonization of the chrysotile cover forming Voronoi tessellation features. (G) Cross section through the entire reaction zone showing the chrysotile cover, a thin layer of oxides, and the lizardite alteration margin down to the etched/notched olivine surface, (H,I) reaction zones containing lizardite and brucite in contact with healthy olivine. (A–D) are for $t = 3$ months (run # 1), (E,G) for $t = 6$ months (run # 2), and (F,H,I) for $t = 12$ months (run # 3).

Serpentinization reaction in NaOH solution was accompanied by the transformation of pre-existing cracks into veins (Figure 4) and the formation of new cracks. Most of the pre-existing cracks were irregular in shape and extended over distances of more than one hundred of micrometres, thus representing preferential pathways for fluid circulation. Extensive reaction zones containing a sizable amount of reaction products were observed at the intersection between the veins and the outer olivine surface, i.e., where the overall surface area exposed to the reaction front was larger. As the reaction proceeded, most of the cracks filled up with serpentine, brucite and accessory minerals such as calcite and magnetite. These minerals were not distributed randomly within the veins but showed obvious phase layering. Brucite typically grew at the interface between serpentine and pristine olivine, as well as in the surface alteration rim, while calcite and magnetite were concentrated in the core layers of the veins. Energy-dispersive X-ray spectroscopy (EDS) analyses showed symmetrical chemical variations from core to rim within the serpentinization products. The core layers were

enriched in incompatible elements, such as Fe and Al, while the Mg content was higher in the rims. Magnetite was Cr- and Ti-rich, a feature frequently reported for progressive maturation of natural serpentine veins [32].

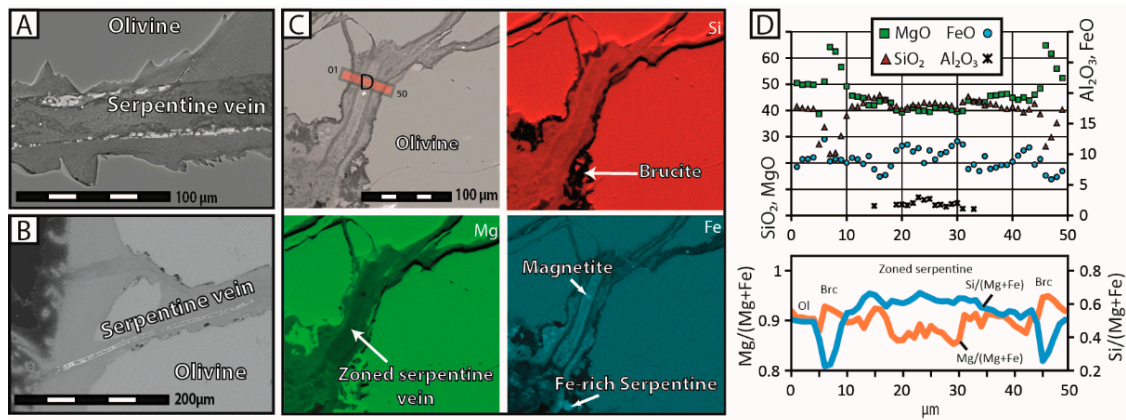


Figure 4. Veins filling pre-existing cracks after reaction in NaOH solution. (A) BSE image displaying obvious mineral zoning between the core and rim layers of the vein, the alteration margins made of lizardite and brucite, and the rough profile of the reaction fronts. (B) BSE image of a vein outlet containing secondary magnetite. (C) EDS elemental maps for Si, Mg and Fe, and (D) chemical profiles corresponding to the red band shown in (C). Fe and Al are enriched in the core layers due to the high content of serpentine, while the presence of brucite in the alteration rim is testified by prominent Mg peaks. (A) is for $t = 6$ months (run # 2), and (B–D) are for $t = 12$ months (run # 3).

In addition to the pre-existing cracks, which were present in the reference olivine grains long before the experiments had started, new cracks formed during the serpentinization process (Figure 5). These usually nucleated at the tips of large dissolution notches, 50–100 μm in width and depth, whether they were located on the outer olivine surface or on the sidewalls of the veins. The most juvenile cracks were short and straight, and stopped abruptly within the olivine bulk. As the reaction progressed, the cracks became longer and wider, and some of them branched to form trident-shaped patterns connected to pre-existing cracks or veins. Thus, according to their respective sizes, shapes, and mutual connectivity, cracks built a hierarchical fracturation network, suggesting a gradual evolution over time. The distribution of new cracks was not uniform throughout the olivine grains. In general, the crack density was at a maximum when in close proximity to pyroxene inclusions, around which they nucleated and propagated radially.

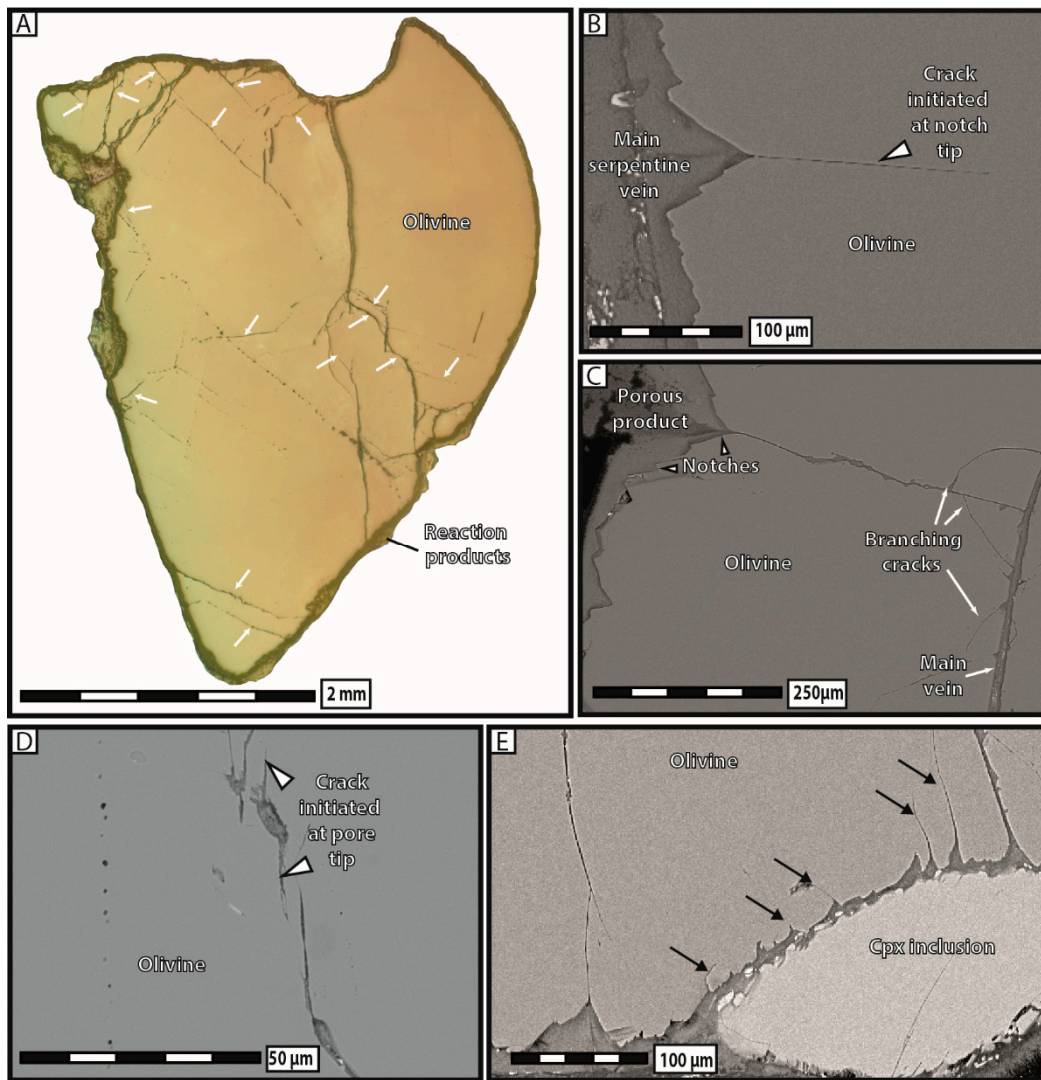


Figure 5. Reflected light micrograph and BSE images of new cracks formed after reaction in NaOH solution. (A) Polished olivine grain with the location of new cracks indicated by white arrows. (B) A short and straight juvenile crack nucleated at the tip of a dissolution notch and vanished within the olivine bulk. (C) More mature cracks showing straight, corrugated, and branched trident-shaped sections ending in a pre-existing vein. (D) Juvenile cracks initiated at the tips of pores filled with reaction products. (E) High density of dissolution notches and newly formed cracks surrounding a clinopyroxene inclusion. (A,D) are for $t = 12$ months (run # 3), and (B,C,E) for $t = 6$ months (run # 2).

Serpentinization in NaOH solution was accompanied by a substantial increase in porosity (Figure 6). Most of the pores were a few micrometres in size, subspherical and empty, and preferentially lined up along microcracks at intervals between 10 and 50 μm . Alternatively, a few of the pores had diameters up to tens of micrometres, forming diamond-shaped cavities that resembled pairs of facing dissolution notches. Some of the pores remained free of reaction products even after long reaction times, while other filled up partly or completely during the reaction. In that latter case, diamond-shaped pores constituted preferential nucleation sites for juvenile cracks, similar to those observed at notch tips. Cracks arising from diamond-shaped pores typically propagated over short distances in the olivine bulk or towards nearby pores, which eventually coalesced to form continuous trails crosscutting the entirety of the olivine grain. Interestingly, a positive correlation could be observed between the size and degree of coalescence of the pores, and the maturity of the cracks, suggesting a concomitant evolution of fracturation and porosity networks over time. The idea that the pore trails observed here

could be previous fluid inclusions streaks [22] or features generated from crack healing [33,34] was considered and may be discarded, as the vast majority of the pores noticed after the experiment were absent in the reference olivine grains. However, we cannot rule out that some of these pores were present in the initial material, even if we did not observe some inside the unreacted grains.

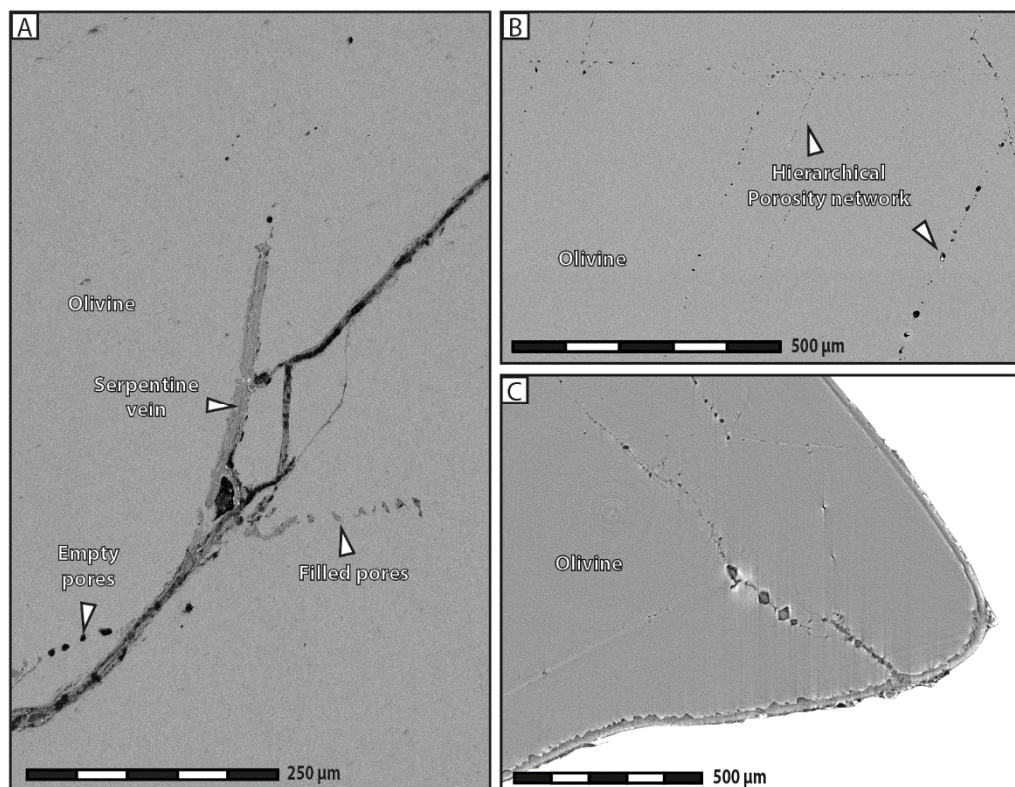


Figure 6. Porosity after reaction in NaOH solution. (A) BSE image of empty and filled pore trails closely related to a serpentine vein. (B) BSE image of the hierarchical porosity network formed by pores of different sizes growing up along microcracks (C) Phase-contrast X-ray synchrotron microtomography image showing tiny spherical pores lining up with large diamond-shaped pores. (A) is for $t = 6$ months (run # 2), and (B,C) for $t = 12$ months (run # 3).

The textures resulting from reaction in NaOH solution were highly comparable to those reported in deionized water (See Supplementary Materials S2). We therefore consider that, apart from the reaction rate, which was substantially higher in NaOH solution, the mechanisms at play were equivalent, thus justifying the use of alkaline solutions to enhance reaction kinetics without compromising the validity of the results.

3.2. Serpentinization Experiments in NaHCO_3 Solution

The most distinctive feature immediately apparent after reaction in NaHCO_3 solution was the pervasive break-up of the starting olivine grains into fragments (Figure 7). This result stood in sharp contrast with the experiments carried out in NaOH solution, for which no such fragmentation behavior was recorded over the duration of the experiments. The number of fragments was typically between 5 and 20, the largest being a few millimeters in size while the smallest hardly exceeded 200 μm . Fragmentation of the olivine grains occurred in all three experimental runs, but with a higher degree of completion as the duration of the reaction increased. In addition to olivine fragmentation, the other feature of interest visible at first glance in all the experiments reacted with NaHCO_3 solution was the widespread scattering of the reaction products. Most of these were piled up in pale-green to reddish polymineralic aggregates dispersed at the bottom of the Teflon capsule or on the olivine surface.

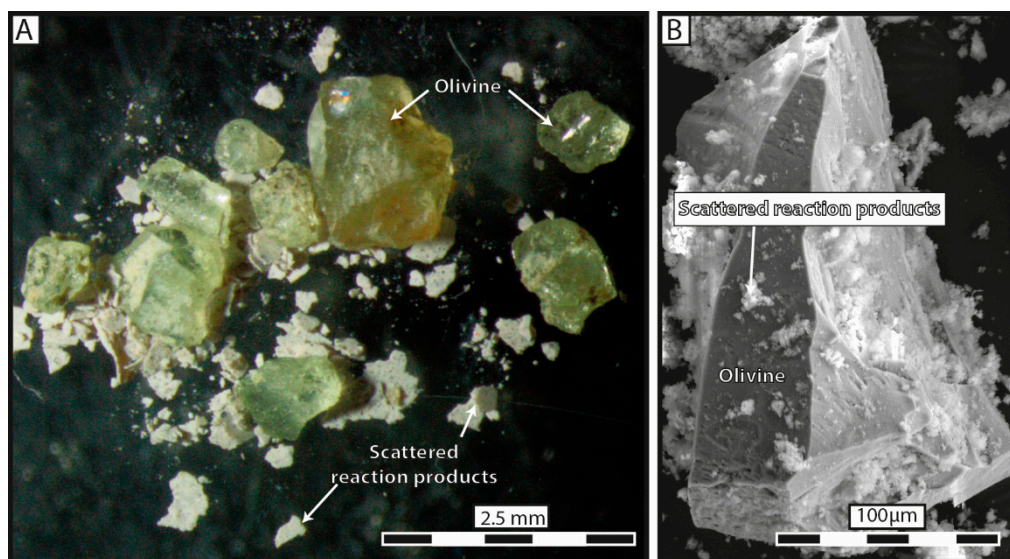


Figure 7. Olivine grains after reaction in NaHCO_3 solution. **(A)** Optical micrograph showing a highly fragmented olivine grain and widespread scattering of the reaction products. **(B)** Secondary electron image displaying small aggregates of reaction products scattered onto an olivine fragment. **(A)** is for $t = 12$ months (run # 3), and **(B)** for $t = 6$ months (run # 2).

Whatever the duration of the experiments, the surface of olivine was free of any form of coherent serpentine cover, such as that observed after reaction in NaOH solution. Surface dissolution features did however occur in the form of leaching strips marked by elongated topographic lows, and closely spaced notches and etch pits (Figure 8). As for reactions in NaOH solution, etching occurred preferentially on specific olivine crystal faces, highlighting the anisotropic nature of dissolution and heterogeneous resistance to weathering. Most of the etch pits displayed a clear tendency to line up and to coalesce as the reaction proceeded.

Aggregates of reaction products were composed of a chaotic mixture of serpentine, magnesite, dolomite, and hematite. The dominant serpentine polymorph was lizardite, as indicated by its bulky crystal habit and Raman spectrum (See Supplementary Materials S3). Chrysotile was rare and never showed the complex textural features observed under similar experimental conditions after reaction in NaOH solution. Carbonates formed euhedral crystals of dolomite and, rarely, magnesite. Hematite usually grew as stacks of platy hexagonal grains and occasionally as stocky minerals. None of the minerals within the aggregates exceeded $20 \mu\text{m}$ in size, except for a few magnesite and dolomite crystals, which occasionally reached sizes of up to $50 \mu\text{m}$.

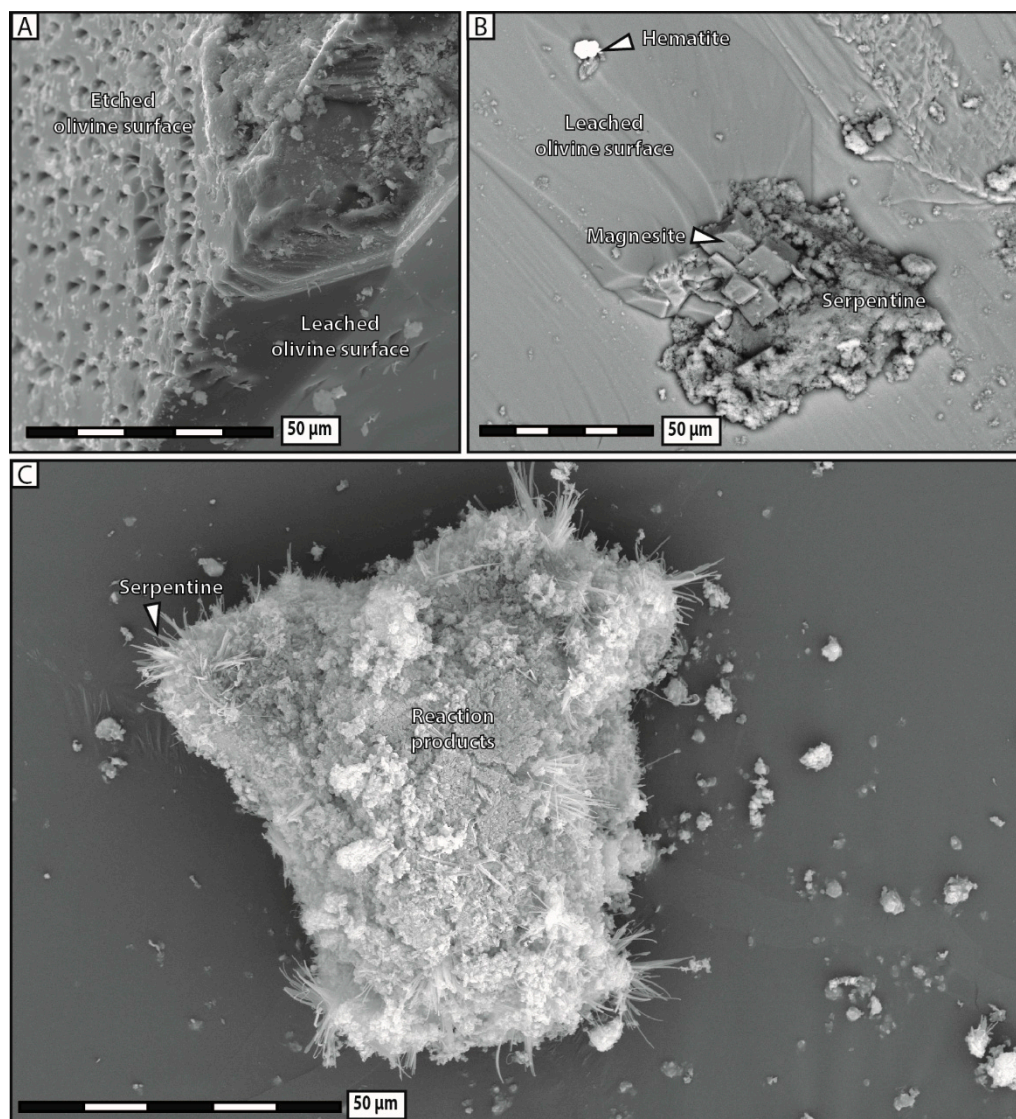


Figure 8. SEM images after reaction in NaHCO_3 solution. (A) Contact zone between etch-pitted and leached olivine surfaces. (B) Cluster of reaction products on top of leached olivine. (C) Single aggregate of reaction products consisting in a mixture of serpentine, magnesite, dolomite and hematite. (B) is for $t = 3$ months (run # 4), and (A and C) for $t = 12$ months (run # 6).

Few major cracks were noticed after reaction in NaHCO_3 solution. Most of them were fresh, i.e., free of reaction products, and lacked the widespread veining observed after reaction in NaOH solution. Occasionally, a few secondary cracks, typically crosscutting the major cracks at high angles, were filled up partly or completely with reaction products. Infilling minerals included serpentine, carbonates and hematite. Alteration features were mostly absent in major cracks but were more numerous on the sidewalls of secondary cracks, in the form of either dissolution notches or diamond-shaped pores (Figure 9).

Porosity was overall higher than after reaction in NaOH solution, especially in the outer $100\ \mu\text{m}$ of olivine grains. Here, pores were oblong or lens-shaped and did not show any correlation with pre-existing cracks. With their non-equant shape and preferred orientation normal to the olivine edge, those pores clearly reflected the anisotropic nature of olivine dissolution. Unlike lens-shaped pores, diamond-shaped pores up to $30\ \mu\text{m}$ in size grew along pre-existing cracks where they lined up to form typical saw-tooth patterns. As for reaction in NaOH solution, only the few diamond-shaped pores filled with reaction products were preferential sites for nucleation and growth of juvenile cracks.

Tiny sub-spherical pores sparsely grew onto microcracks too, but to a much lower extent than after reaction in NaOH solution. No evidence for a hierarchical porosity network was observed.

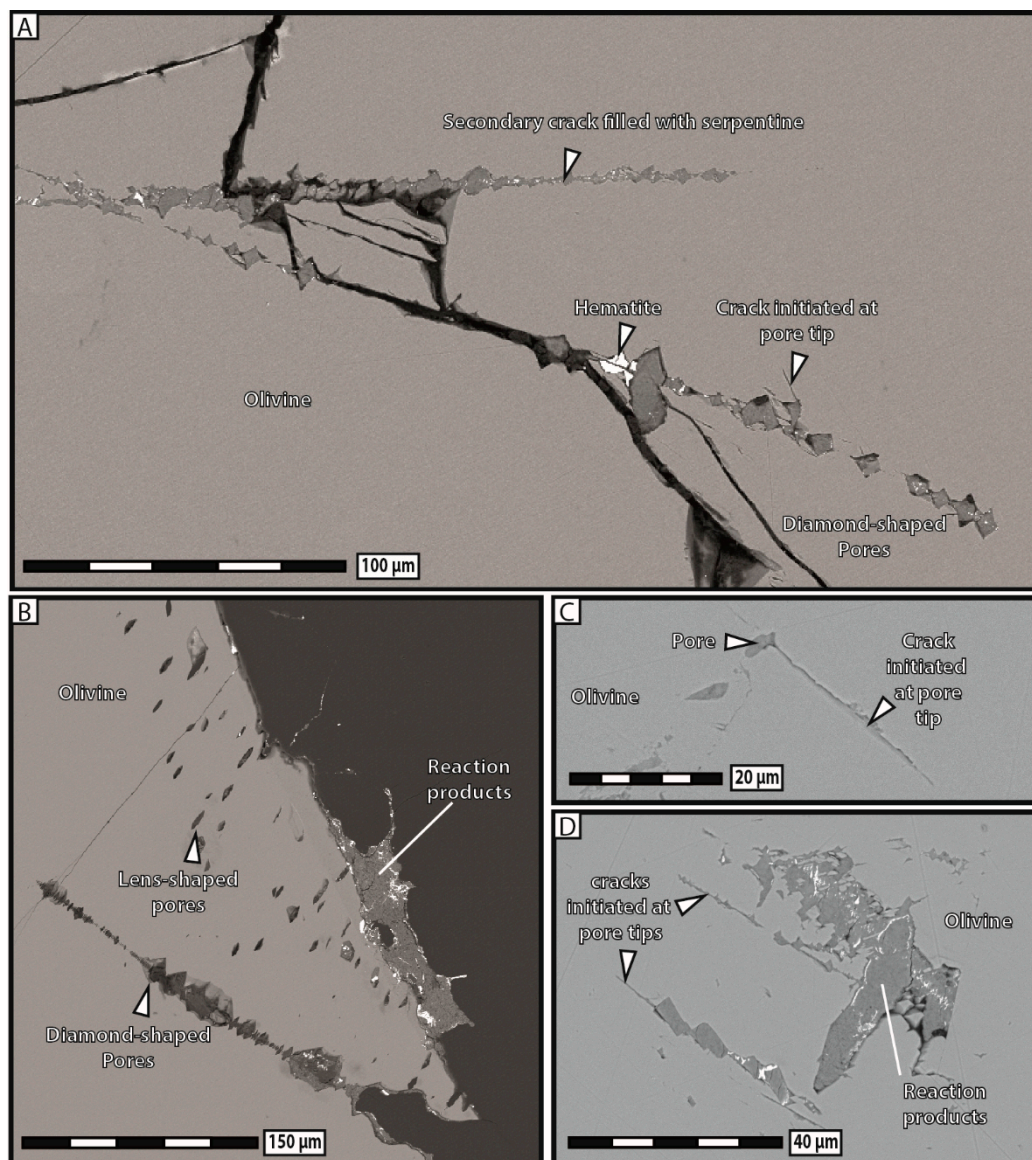


Figure 9. BSE images of porosity features after reaction in NaHCO_3 solution. (A) Diamond-shaped pores filled with reaction products and lining up along secondary cracks. (B) Oblong and lens-shaped pores scattered in the outer parts of olivine grains. Some pores were filled with reaction products while other have remained empty. (C,D) Juvenile cracks initiated at the tips of diamond-shaped pores filled with reaction products. (A,B) are for $t = 6$ months (run # 5), and (C,D) for $t = 12$ months.

4. Discussion

4.1. Coupled vs. Decoupled Dissolution-Precipitation

Serpentinization experiments carried out in alkaline NaOH and NaHCO_3 solutions revealed strikingly different macro- and microscopic textures (Figure 10). During reaction in NaOH solution, olivine grains remained whole—as previously reported for smaller grain fraction [24]—and the reaction products precipitated in-situ, either as infilling material within pre-existing and new cracks or as a coherent cover onto the olivine surface. The extent of grain fracturation increased significantly, as the reaction proceeded mainly through intracrystalline reaction-induced cracking, and a hierarchical

porosity network formed due to the progressive growth and coalescence of pores along microcracks. In contrast, olivine grains reacted in NaHCO_3 solution systematically broke apart into several fragments and most of the reaction products precipitated in aggregates widely scattered away from dissolution sites. Substantial porosity developed across olivine grains and no reaction-induced cracking occurred, except at the tips of the very few diamond-shaped pores filled with reaction products.

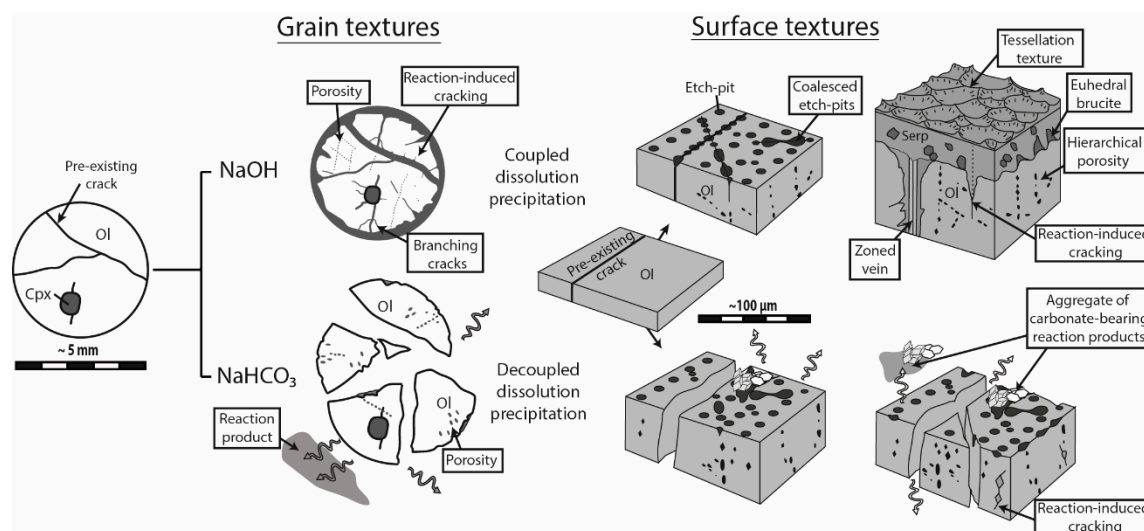


Figure 10. Sketch summarizing the distinct grain and surface features observed after reaction in NaOH and NaHCO_3 solutions. Note the very different degree of spatial coupling between dissolution and precipitation in each reaction type Cpx: clino-pyroxene, Ol: olivine, Serp: serpentine.

Our experimental data indicate a very different degree of coupling between dissolution and precipitation processes, depending on whether they have occurred in carbon dioxide-free (NaOH) or carbon dioxide-rich (NaHCO_3) solutions. In the former, dissolution of olivine and precipitation of the reaction products are intimately correlated, as they occur concomitantly and with minimum mass transfer, while in the latter, precipitation mainly takes place away from dissolution sites, thus indicating clear spatial decoupling between both processes. The reason for such a distinct reaction mechanism is still unclear, but it is surely not a consequence of the difference in alkalinity between the two reactive solutions. The reference experiment run in deionized water ($\text{pH}_{\text{start}} = 5.8$) displays no decoupling between dissolution and precipitation (see Supplementary Materials S2). It has therefore closer similarities with the experiments carried out in highly alkaline NaOH solution ($\text{pH}_{\text{start}} = 13.5$), than with those conducted in mildly alkaline NaHCO_3 solution ($\text{pH}_{\text{start}} = 8.7$). Consequently, while the respective pH values can explain to some extent the different reaction rates in two types of experiments, they cannot account for the discrepant dissolution–precipitation behavior observed here.

A possible explanation for the distinct degree of coupling between dissolution and precipitation could be the disequilibrium between the respective rates of precipitation and fluid flow [13]. In a situation in which precipitation is sluggish and slow, as expected for carbonate minerals [35], fluid flow and transport of chemical species may overtake crystal growth. The high chemical potential between the crack interfaces and the precipitation sites would sustain the constant removal of the reaction products, and shift precipitation far away from dissolution sites. In contrast, a high precipitation and growth rate of the reaction products, such as that of brucite and serpentine during hydration experiments, triggers veining and partial clogging of the circulation pathways. Consequently, fluid flow and mass transfer capabilities may drop down drastically, which further favors in-situ precipitation. This interpretation is well in line with the recent experimental work of Malvoisin and Brunet (2014) on sintered olivine aggregates [28], who reported that the nucleation and growth of brucite directly onto the olivine surface is kinetically favored by the system, as it minimizes surface energy. We therefore consider that the rapid growth of brucite and serpentine has a local inhibitory

effect on fluid flow, leaving the reaction products with no other option but to precipitate in situ. In contrast, the sluggishness of carbonate precipitation can keep pre-existing fluid circulation pathways open over long periods, sustaining efficient mass transport, and therefore, delocalized precipitation.

The clear-cut results reported here have far-reaching consequences on the way the massive increase in volume accompanying serpentinization reactions is accommodated. A high degree of spatial coupling between dissolution and precipitation implies that the volumetric changes have to be fitted in-situ, e.g., through reaction-induced cracking, otherwise the reaction will stop. In contrast, when both mechanisms are spatially decoupled, the increase in volume is compensated for through long-range transportation of the reaction products. The fact that carbonation tends to prioritize mass transfer is not anecdotal, as the reaction is mostly self-driven and likely to persist over time. This positive loop, in which the constant removal of the reaction products enhances rock permeability, and therefore fluid flow and mass transfer, suggests that the presence of carbon dioxide in the reactive fluids facilitates the widespread dispersal of the reaction products and the redistribution of chemical elements within the oceanic lithosphere. This process leads to sharp mineralogical and chemical dissociation between the parent rock and the carbonated reaction products, as illustrated by the textures of natural ophicarbonates [11,36–38]. The pervasive break-up of the olivine grains observed after the carbonation experiments can be interpreted as a low-pressure analogue for the intensely brecciated textures commonly reported for natural ophicarbonates found at the top of serpentinite units [39–42], even where no significant tectonic activity is invoked. In both cases, fragmentation can be easily explained by the lack of cohesion commonly provided by veins, in which serpentine acts as a glue, welding olivine fragments together.

4.2. Reaction-Induced Cracking

Our experimental data have provided ample evidence for the formation of new intracrystalline cracks during serpentinization. These results are in good agreement with those reported in natural serpentinites by other authors [9,21], who proposed that the nucleation and propagation of new cracks is driven by the crystallization stress accumulated at the tips of dissolution notches during progressive serpentinization [43,44]. We therefore support the idea that the large increase in volume associated with phase transformation does not necessarily impede the extent of serpentinization reactions, but rather triggers the formation of a hierarchical fracturation network allowing for serpentinization to continue during hydration. The fact that reaction-induced cracking is abundant in hydration experiments, i.e., reactions in which no long-range mass transfer and no spatial decoupling between dissolution and precipitation have occurred, indicates that, at least in serpentinite systems, in-situ precipitation of the reaction products is a prerequisite to raise stress at notch tips and trigger mineral/rock fracturation. This point is further evidenced in our carbonation reactions, in which only the diamond-shaped pores filled with reaction products have generated new cracks. Consequently, our experimental work unequivocally argues for a cause-and-effect relationship linking in-situ phase transformation and intracrystalline reaction-induced cracking whatever the reaction (hydration or carbonation). The striking similarities between the reaction-induced cracks observed experimentally here and in natural ophiolites give further credence to this hypothesis.

There is little doubt that if the reaction products had massively precipitated in situ during our carbonation experiments, substantially more reaction-induced cracking, similar to that observed after hydration experiments, would have taken place in that case too. Indeed, carbonation in no way constitutes an intrinsic obstacle to reaction-induced cracking, as long as dissolution and precipitation mechanisms are spatially coupled and dominant over mass transfer. This finding leads us to stress that a high degree of spatial coupling between dissolution and precipitation constitutes an essential condition for reaction-induced cracking, much more than the type of reaction itself, at least when the confining pressure is very low. However, carbonation reactions show a weaker tendency for in situ precipitation, and consequently also, reaction-induced cracking rather, than hydration reactions. Alternatively, carbonation reactions could also give rise to delayed reaction-induced cracking occurring

in the nearby rocks where precipitation takes place, but our experiments on single grains did not allow for such observations.

It is worth noting that, in our experiments, cracking has been locally enhanced by the occurrence of less-reactive mineral inclusions of pyroxene or spinel. This process is common and has been widely reported in the literature for natural peridotites [32,45]. Pyroxene and spinel are highly resistant to alteration and act as hard spots around which stress accumulates and radial cracks nucleate. This effect may be further amplified by the high serpentinization efficiency attributed to a greater silica activity at the olivine-pyroxene boundary [46]. We therefore conclude that natural, inclusion-rich olivine grains and peridotites may be more prone to intracrystalline reaction-induced cracking than monomineralic rocks or manufactured samples of dunite sintered from synthetic olivine powder.

4.3. Porosity, an Alternative and Complementary Way for Reaction Propagation

Our experimental data indicate that the development of porosity is an essential aspect of serpentinization reactions, whatever the composition of the reactive fluid. As a general trend, our results show that the apparent pore abundance is positively correlated with fracturation, in the sense that highly fractured grains contain more pores than less fractured ones in hydration experiments. Moreover, we have proposed several lines of evidence to demonstrate that porosity and fracturation networks tend to mutually self-propagate in the course of the reaction. The observation that pores preferably line up along microcracks indicates that fracturation actively participates in spreading porosity towards the interior of olivine grains. The fact that juvenile cracks obviously nucleate at the tips of diamond-shaped pores shows that the reverse is also true, i.e., that pores play an equally important role in the propagation of the fracture network. This self-reinforcing loop, in which more cracks generate more pores, and vice versa, is noteworthy, as it guarantees efficient progression of the reaction front through the olivine grains, and therefore the survival of serpentinization reactions over time in a context of massive volume increase and limited mass transfer.

Besides highlighting the strong mutual correlation between porosity and fracturation, during both hydration and carbonation, our experimental results suggest that some form of porosity may develop in absence of cracks too. The growth of isolated pores in the outer fringes of olivine grains during carbonation experiments indicates that fracturation is not an absolute requirement for pore formation. According to this view, porosity is thought to propagate spontaneously, e.g., in response to high chemical gradients between dissolution and precipitation sites. Alternatively, those pores could also be 2D cross-sectional views of dissolution channels, similar to those recently reported by Xing et al. [21]. Whatever the interpretation, the occurrence of porosity features disconnected from cracks—in good agreement with previous studies [47,48]—is not irrelevant, as it suggests that serpentinization could, to some extent, take place with little or no fracturation at all. This result stresses the multivalent nature of serpentinization, which can follow alternative reaction paths to keep progressing over time.

Finally, the coexistence of pores filled with reaction products immediately adjacent to empty pores suggests that serpentinization continuously creates and eliminates porosity, in accordance with the physicochemical conditions at a specific time and place. It must be noted that both filled and empty pores can positively influence the course of serpentinization reactions. While empty pores facilitate fluid flow and mass transfer, pores filled with reaction products participate in the spreading of the fracturation network through reaction-induced cracking. This observation was already noted in other studies [49,50].

5. Implications and Conclusions

In the present study, hydration and carbonation experiments were carried out on coarse olivine grains in order to better understand the processes at play during serpentinization reactions. The striking parallels that can be drawn between the textural features observed here and in natural outcrops are excellent indicators of the relevance of the experimental set-up and starting materials. The tendency of hydrated olivine grains to accommodate the reaction products in situ while remaining

whole is characterized in hydrated peridotites by the widespread occurrence of mesh texturing and veining. In contrast, the delocalized precipitation of the reaction products and the pervasive break-up of olivine grains after carbonation reactions is in good agreement with the bimodal mineral distribution and the highly brecciated and often chaotic nature of many ophicarbonates. We therefore concluded that the fluid composition, and in particular the carbon dioxide content of the volatile phase, not only determines the mineral species occurring in the reaction products, but also drastically controls the textures of serpentinized rocks and the degree of redistribution of the chemical elements in the oceanic lithosphere.

Our study has provided the first experimental evidence for a cause-and-effect relationship between in situ precipitation and intracrystalline reaction-induced cracking in olivine especially during hydration experiments. We have shown that this process occurs regardless of the type of reactive fluid, commencing as soon as precipitation of the reaction products occurs in situ and exerts a sufficient differential stress at the tips of dissolution notches or pores. This finding is particularly timely, as two very recent experimental serpentinization studies have questioned the very existence of such a feature at the expense of intercrystalline reaction-induced cracking [13,21]. Based on our own experimental results and observations, however, we strongly advocate that intracrystalline reaction-induced cracking does occur in olivine, and that it is an essential component of rock fracturation during serpentinization reactions.

Finally, our study has highlighted the extreme versatility and multi-faceted nature of serpentinization. Processes that could at first be misidentified as detrimental, such as massive volume increase during phase transformations and ensuing pore clogging, are in reality not major obstacles for the continuation of serpentinization reactions, due to the ability of the system to adapt through a series of positive loops, making it resilient and enduring over time. Among the most striking features are the paired and concomitant development of fracturation and porosity networks, and the possibility to extend (or reduce) porosity even in absence of fracturation. The many strings serpentinization has to its bow undoubtedly explains at least part of its considerable success over time and the widespread occurrence of fully serpentinized rocks in very different geological contexts all over the world.

Supplementary Materials: The following are available online at <http://www.mdpi.com/2075-163X/8/9/412/s1>. Supplementary Material S1: Field emission electron probe microanalyzer (FE-EPMA) chemical characterization of starting olivine grains. Supplementary Material S2: Experimental setup and Olivine serpentinization in deionized water. Supplementary Material S3: Identification of serpentine polymorphs using Raman spectroscopy.

Author Contributions: R.L. prepared the samples, established the experimental protocol, characterized the reaction products, and took the lead in the interpretation of the data. G.M.-H. supervised the serpentinization experiments and collected the reaction product. F.R. performed the X-ray synchrotron microtomography analyses and post-processing. P.V. collaborated in the acquisition of scanning electron microscopy data and participated in writing the manuscript. All authors contributed to the scientific interpretation of the data.

Funding: The free access to lab facilities was made available by the Universities of Lausanne (Switzerland) and Grenoble Alpes (France). F.R. acknowledges funding from the Norwegian Research Council (grant HADES 250661).

Acknowledgments: We are grateful to Martin Robyr for his help during the electron probe microanalyses, and to Deyanira Cisneros-Lazaro for proofreading the last version of the manuscript.

Conflicts of Interest: The authors declare no conflicts of interest.

References

1. Hirth, G.; Guillot, S. Rheology and tectonic significance of serpentinite. *Elements* **2013**, *9*, 107–113. [[CrossRef](#)]
2. Deschamps, F.; Guillot, S.; Godard, M.; Andreani, M.; Hattori, K. Serpentinites act as sponges for Fluid-Mobile-Elements in abyssal and subduction zone environments. *Terra Nova* **2011**, *23*, 171–178. [[CrossRef](#)]
3. Kelemen, P.B.; Matter, J. In situ carbonation of peridotite for CO₂ storage. *Proc. Natl. Acad. Sci. USA* **2008**, *105*, 17295–17300. [[CrossRef](#)]
4. Seifritz, W. CO₂ disposal by means of silicates. *Nature* **1990**, *345*, 486. [[CrossRef](#)]
5. McCollom, T.M.; Bach, W. Thermodynamic constraints on hydrogen generation during serpentinization of ultramafic rocks. *Geochim. Cosmochim. Acta* **2009**, *73*, 856–875. [[CrossRef](#)]

6. Coleman, R.; Keith, T. A chemical study of serpentinization—Burro Mountain, California. *J. Petrol.* **1971**, *12*, 311–328. [[CrossRef](#)]
7. O’Hanley, D.S. Solution to the volume problem in serpentinization. *Geology* **1992**, *20*, 705–708. [[CrossRef](#)]
8. Andreani, M.; Luquot, L.; Gouze, P.; Godard, M.; Hoise, E.; Gibert, B. Experimental study of carbon sequestration reactions controlled by the percolation of CO₂-rich brine through peridotites. *Environ. Sci. Technol.* **2009**, *43*, 1226–1231. [[CrossRef](#)] [[PubMed](#)]
9. Peuble, S.; Andreani, M.; Godard, M.; Gouze, P.; Barou, F.; Van de Moortele, B.; Mainprice, D.; Reynard, B. Carbonate mineralization in percolated olivine aggregates: Linking effects of crystallographic orientation and fluid flow. *Am. Mineral.* **2015**, *100*, 474–482. [[CrossRef](#)]
10. Tutolo, B.M.; Mildner, D.F.; Gagnon, C.V.; Saar, M.O.; Seyfried, W.E. Nanoscale constraints on porosity generation and fluid flow during serpentinization. *Geology* **2016**, *44*, 103–106. [[CrossRef](#)]
11. Boschi, C.; Früh-Green, G.L.; Delacour, A.; Karson, J.A.; Kelley, D.S. Mass transfer and fluid flow during detachment faulting and development of an oceanic core complex, Atlantis Massif (MAR 30 N). *Geochem. Geophys. Geosyst.* **2006**, *7*, Q01004. [[CrossRef](#)]
12. Macdonald, A.; Fyfe, W. Rate of serpentinization in seafloor environments. *Tectonophysics* **1985**, *116*, 123–135. [[CrossRef](#)]
13. Zhu, W.; Fousseis, F.; Lisabeth, H.; Xing, T.; Xiao, X.; De Andrade, V.; Karato, S. Experimental evidence of reaction-induced fracturing during olivine carbonation. *Geophys. Res. Lett.* **2016**, *43*, 9535–9543. [[CrossRef](#)]
14. Rouméjon, S.; Cannat, M.; Agrinier, P.; Godard, M.; Andreani, M. Serpentinization and fluid pathways in tectonically exhumed peridotites from the Southwest Indian Ridge (62–65 E). *J. Petrol.* **2015**, *56*, 703–734. [[CrossRef](#)]
15. Wicks, F.; Whittaker, E. Serpentine textures and serpentinization. *Can. Mineral.* **1977**, *15*, 459–488.
16. Lisabeth, H.; Zhu, W.; Kelemen, P.; Ilgen, A. Experimental evidence for chemo-mechanical coupling during carbon mineralization in ultramafic rocks. *Earth Planet. Sci. Lett.* **2017**, *474*, 355–367. [[CrossRef](#)]
17. Malvoisin, B.; Brunet, F.; Carlut, J.; Rouméjon, S.; Cannat, M. Serpentinization of oceanic peridotites: 2. Kinetics and processes of San Carlos olivine hydrothermal alteration. *J. Geophys. Res. Solid Earth* **2012**, *117*, B04102. [[CrossRef](#)]
18. Demartin, B.; Hirth, G.; Evans, B. Experimental constraints on thermal cracking of peridotite at oceanic spreading centres. *Ocean Ridges* **2004**, *148*, 167–185.
19. Escartin, J.; Hirth, G.; Evans, B. Effects of serpentinization on the lithospheric strength and the style of normal faulting at slow-spreading ridges. *Earth Planet. Sci. Lett.* **1997**, *151*, 181–189. [[CrossRef](#)]
20. Peuble, S.; Andreani, M.; Gouze, P.; Pollet-Villard, M.; Reynard, B.; Van de Moortele, B. Multi-scale characterization of the incipient carbonation of peridotite. *Chem. Geol.* **2018**, *476*, 150–160. [[CrossRef](#)]
21. Xing, T.; Zhu, W.; Fousseis, F.; Lisabeth, H. Generating porosity during olivine carbonation via dissolution channels and expansion cracks. *Solid Earth* **2018**, *9*, 879–896. [[CrossRef](#)]
22. Luhmann, A.J.; Tutolo, B.M.; Bagley, B.C.; Mildner, D.F.; Scheuermann, P.P.; Feinberg, J.M.; Ignatyev, K.; Seyfried, W.E., Jr. Chemical and physical changes during seawater flow through intact dunite cores: An experimental study at 150–200 °C. *Geochim. Cosmochim. Acta* **2017**, *214*, 86–114. [[CrossRef](#)]
23. Klein, F.; Grozeva, N.G.; Seewald, J.S.; McCollom, T.M.; Humphris, S.E.; Moskowitz, B.; Berquó, T.S.; Kahl, W.-A. Experimental constraints on fluid-rock reactions during incipient serpentinization of harzburgite. *Am. Mineral.* **2015**, *100*, 991–1002. [[CrossRef](#)]
24. Lafay, R.; Montes-Hernandez, G.; Janots, E.; Chiriac, R.; Findling, N.; Toche, F. Mineral replacement rate of olivine by chrysotile and brucite under high alkaline conditions. *J. Cryst. Growth* **2012**, *347*, 62–72. [[CrossRef](#)]
25. Martin, B.; Fyfe, W. Some experimental and theoretical observations on the kinetics of hydration reactions with particular reference to serpentinization. *Chem. Geol.* **1970**, *6*, 185–202. [[CrossRef](#)]
26. Malvoisin, B.; Brunet, F. Water diffusion-transport in a synthetic dunite: Consequences for oceanic peridotite serpentinization. *Earth Planet. Sci. Lett.* **2014**, *403*, 263–272. [[CrossRef](#)]
27. Grozeva, N.G.; Klein, F.; Seewald, J.S.; Sylva, S.P. Experimental study of carbonate formation in oceanic peridotite. *Geochim. Cosmochim. Acta* **2017**, *199*, 264–286. [[CrossRef](#)]
28. Moody, J.B. Serpentinization: A review. *Lithos* **1976**, *9*, 125–138. [[CrossRef](#)]
29. Lafay, R.; Montes-Hernandez, G.; Janots, E.; Chiriac, R.; Findling, N.; Toche, F. Simultaneous precipitation of magnesite and lizardite from hydrothermal alteration of olivine under high-carbonate alkalinity. *Chem. Geol.* **2014**, *368*, 63–75. [[CrossRef](#)]

30. Klein, F.; Garrido, C.J. Thermodynamic constraints on mineral carbonation of serpentinized peridotite. *Lithos* **2011**, *126*, 147–160. [[CrossRef](#)]
31. Weaire, D.; Kermode, J.; Wejchert, J. On the distribution of cell areas in a Voronoi network. *Philos. Mag. B* **1986**, *53*, L101–L105. [[CrossRef](#)]
32. Schwarzenbach, E.M.; Caddick, M.J.; Beard, J.S.; Bodnar, R.J. Serpentinization, element transfer, and the progressive development of zoning in veins: Evidence from a partially serpentinized harzburgite. *Contrib. Mineral. Petrol.* **2016**, *171*, 5. [[CrossRef](#)]
33. Wanamaker, B.; Wong, T.; Evans, B. Decrepitation and crack healing of fluid inclusions in San Carlos olivine. *J. Geophys. Res. Solid Earth* **1990**, *95*, 15623–15641. [[CrossRef](#)]
34. Smith, D.L.; Evans, B. Diffusional crack healing in quartz. *J. Geophys. Res. Solid Earth* **1984**, *89*, 4125–4135. [[CrossRef](#)]
35. Xu, J.; Yan, C.; Zhang, F.; Konishi, H.; Xu, H.; Teng, H.H. Testing the cation-hydration effect on the crystallization of Ca–Mg–CO₃ systems. *Proc. Natl. Acad. Sci. USA* **2013**, *110*, 17750–17755. [[CrossRef](#)] [[PubMed](#)]
36. Surour, A.A.; Arafa, E.H. Ophicarbonates: Calichified serpentinites from Gebel Mohagara, Wadi Ghadir area, Eastern Desert, Egypt. *J. Afr. Earth Sci.* **1997**, *24*, 315–324. [[CrossRef](#)]
37. Clerc, C.; Boulvais, P.; Lagabrielle, Y.; de Saint Blanquat, M. Ophicalcites from the northern Pyrenean belt: A field, petrographic and stable isotope study. *Int. J. Earth Sci.* **2014**, *103*, 141–163. [[CrossRef](#)]
38. Lemoine, M.; Bourbon, M.; de Graciansky, P.-C.; Letolle, R. Isotopes du carbone et de l'oxygène de calcaires associés à des ophiolites (Alpes occidentales, Corse, Appennin): Indices possibles d'un hydrothermalisme océanique téthysien. *Rev. Géogr. Phys. Géol. Dyn.* **1983**, *24*, 305–314.
39. Tartarotti, P.; Festa, A.; Benciolini, L.; Balestro, G. Record of Jurassic mass transport processes through the orogenic cycle: Understanding chaotic rock units in the high-pressure Zermatt-Saas ophiolite (Western Alps). *Lithosphere* **2017**, *9*, 399–407. [[CrossRef](#)]
40. Bernoulli, D.; Weissert, H. Sedimentary fabrics in Alpine ophicalcites, south Pennine Arosa zone, Switzerland. *Geology* **1985**, *13*, 755–758. [[CrossRef](#)]
41. Früh-Green, G.L.; Weissert, H.; Bernoulli, D. A multiple fluid history recorded in Alpine ophiolites. *J. Geol. Soc.* **1990**, *147*, 959–970. [[CrossRef](#)]
42. Früh-Green, G.L.; Kelley, D.S.; Bernasconi, S.M.; Karson, J.A.; Ludwig, K.A.; Butterfield, D.A.; Boschi, C.; Proskurowski, G. 30,000 years of hydrothermal activity at the Lost City vent field. *Science* **2003**, *301*, 495–498. [[CrossRef](#)] [[PubMed](#)]
43. Plümpner, O.; Røyne, A.; Magrasó, A.; Jamtveit, B. The interface-scale mechanism of reaction-induced fracturing during serpentinization. *Geology* **2012**, *40*, 1103–1106. [[CrossRef](#)]
44. Rudge, J.F.; Kelemen, P.B.; Spiegelman, M. A simple model of reaction-induced cracking applied to serpentinization and carbonation of peridotite. *Earth Planet. Sci. Lett.* **2010**, *291*, 215–227. [[CrossRef](#)]
45. Malvoisin, B.; Brantut, N.; Kaczmarek, M.-A. Control of serpentinisation rate by reaction-induced cracking. *Earth Planet. Sci. Lett.* **2017**, *476*, 143–152. [[CrossRef](#)]
46. Ogasawara, Y.; Okamoto, A.; Hirano, N.; Tsuchiya, N. Coupled reactions and silica diffusion during serpentinization. *Geochim. Cosmochim. Acta* **2013**, *119*, 212–230. [[CrossRef](#)]
47. Lisabeth, H.; Zhu, W.; Xing, T.; De Andrade, V. Dissolution assisted pattern formation during olivine carbonation. *Geophys. Res. Lett.* **2017**, *44*. [[CrossRef](#)]
48. Merino, E.; Ortoleva, P.; Strickholm, P. Generation of evenly-spaced pressure-solution seams during (late) diagenesis: A kinetic theory. *Contrib. Mineral. Petrol.* **1983**, *82*, 360–370. [[CrossRef](#)]
49. Kelemen, P.B.; Hirth, G. Reaction-driven cracking during retrograde metamorphism: Olivine hydration and carbonation. *Earth Planet. Sci. Lett.* **2012**, *345*, 81–89. [[CrossRef](#)]
50. Hövelmann, J.; Austrheim, H.; Beinlich, A.; Munz, I.A. Experimental study of the carbonation of partially serpentinized and weathered peridotites. *Geochim. Cosmochim. Acta* **2011**, *75*, 6760–6779. [[CrossRef](#)]

